

# Bistability and nonequilibrium transitions in the optically polarized system of cavity polaritons under nanosecond-long resonant excitation

S. S. Gavrilov,\* A. S. Brichkin, A. A. Demenev, A. A. Dorodnyy, S. I. Novikov, and V. D. Kulakovskii  
*Institute of Solid State Physics, RAS, Chernogolovka 142432, Russia*

S. G. Tikhodeev  
*A. M. Prokhorov General Physics Institute, RAS, Moscow 119991, Russia*

N. A. Gippius  
*A. M. Prokhorov General Physics Institute, RAS, Moscow 119991, Russia and  
 LASMEA, UMR 6602 CNRS, Université Blaise Pascal, 63177 Aubière, France*  
 (Dated: November 11, 2018)

The polarization dependence of nonequilibrium transitions in a multistable cavity-polariton system is studied under a nanosecond long resonant optical excitation at the normal and magic angle incidences with various polarizations of the pump beam. The temporal correlations between the frequency, intensity, and optical polarization of the intra-cavity field, which all undergo sharp threshold-like changes due to the spin dependent interaction of cavity polaritons, are visualized. The observed dynamics cannot be reproduced within the conventional semi-classical model based on the Gross-Pitaevskii equations. To explain the observed phenomena, it is necessary to take into account the unpolarized exciton reservoir which brings on additional blueshift of bright excitons, equal in the  $\sigma^+$  and  $\sigma^-$  polarization components. This model explains the effect of polarization instability under both pulsed and continuous wave resonant excitation conditions, consistently with the spin ring pattern formation that has recently been observed under Gaussian shaped excitation.

PACS numbers: 71.36.+c, 42.65.Pc, 42.55.Sa

## I. INTRODUCTION

Cavity polaritons are bound light-matter states that appear due to the strong coupling of 2D excitons and photons in semiconductor microcavities.<sup>1,2</sup> The optically driven system of polaritons behaves like a weakly imperfect Bose gas, which results in a spectacular row of polariton collective phenomena such as multistability,<sup>3-5</sup> parametric scattering,<sup>6-8</sup> pattern formation,<sup>9,10</sup> self-organization effects,<sup>11,12</sup> dynamical Bose-Einstein condensation.<sup>13</sup> Polariton multistability attracts much attention as a potential candidate for very fast picosecond range optical switching on a micron size scale.<sup>14,15</sup> Moreover, the sharp transitions in intra-cavity field, stemming from the multistability, can proceed concurrently with inter-mode parametric scattering, which determines interesting ways of polariton self-organization under pumping near the inflection point of the lower polariton branch (the “magic angle”).<sup>8,11,12</sup>

The polariton bistability has recently been studied in the “scalar” approximation neglecting the spin degrees of freedom.<sup>3,8</sup> Because of the mutual interaction of polaritons, their energy effectively depends on the intra-cavity field magnitude. The repulsion between excitons leads to the blueshift of polariton energy. When the pump is itself blue-detuned from the polariton resonance, a strong positive feedback loop between the resonance energy and the field amplitude is created in a certain range of system parameters, resulting in sharp jumps in the intra-cavity field and, hence, in the cavity transmission. Consequently, the transmission signal can exhibit a promi-

nent hysteresis in the dependence on continuous-wave (cw) pump intensity.<sup>3,8</sup>

The response of the optically excited polariton system becomes more complicated with allowance made for exciton spin degrees of freedom (that corresponds to arbitrary optical polarization of the intra-cavity field). In the general case the system has up to four stable states under a given cw pump, whereas the actual state of the system is determined by the history of the excitation process.<sup>4,16</sup> In critical points, where a number and/or stability of stationary solutions change, the system can exhibit sharp jumps in both the amplitude and polarization of the intra-cavity field. Under a spatially inhomogeneous (e.g., Gaussian shaped) cw excitation the system can also exhibit a nontrivial spatial distribution of polarization of the luminescence signal, like the “spin ring” patterns,<sup>14</sup> due to the same underlying phenomena.

The strong multistability effect predicted in Ref. 4 has recently been observed experimentally,<sup>5</sup> including the sharp jumps in the cavity transmission under a smooth variation of the pump polarization degree. The spin ring patterns under Gaussian shaped excitation have also been reported.<sup>17,18</sup> All these experiments were carried out under the cw excitation. Thus, one of the still remaining questions is the dynamical peculiarities of the transitions in a multistable system, which could only be traced using the time-resolved techniques. Particularly, the characteristic switching times between different stability branches call for the experimental study, for they can have a crucial impact upon the practical implementations.

Another question concerns the theoretical approach allowing to describe the observed multistability effect in microcavities. Traditionally, the multistability is considered in terms of the self-acting classical fields corresponding to macro-occupied coherent polariton modes which appear under a coherent resonant excitation.<sup>3,4,14,15</sup> Although such an approach is supposed to be sufficient to describe the bistability in a circularly polarized system,<sup>3</sup> it gives wrong predictions for the general case of elliptically polarized excitation.<sup>19</sup> Most probably, the incoherent states of the exciton reservoir which are inevitably excited in optical experiments have a substantial impact on the decay rates and energies of polaritons. For instance, the nonlinear decay of polaritons with different circular polarizations was taken into consideration in order to explain the experimental data in Ref. 5. Further, the nonequilibrium transitions reported in Ref. 17 can only be reproduced in calculations taking into account the reservoir induced shifts of the polariton energy.

In the present work we report the experimental study of nonequilibrium transitions in the multistable cavity polariton system. Unlike in recent Refs. 5, 17, and 18, we have studied the optically polarized system under a pulsed nanosecond-long excitation, which allowed us to trace the time-resolved dynamics of the intra-cavity field. The shifts in polariton energy were reflected by temporal variations in the transmission energy spectrum. Thus, the employed technique is capable of visualizing the temporal correlations between the resonance energy and intensity of the intra-cavity field.

We discuss in detail the time dependence of the transmission signal polarization, below as well as above the threshold, for several polarizations of the pump beam. The observed polarization behavior cannot be reproduced within a semi-classical model based on the Gross-Pitaevskii equations considered in Refs. 4, 14, and 16. The experimental results allowed us to develop a phenomenological model to describe a multistable polariton system with a proper regard to the exciton reservoir. The reservoir excitons shift the polariton energy that, in turn, influences the thresholds of nonequilibrium transitions. Both the linear and nonlinear mechanisms of exciton scattering into the reservoir are found to be significant within a sub-nanosecond time scale. While the nonlinear decay of cross-circularly polarized excitons leads to the levelling of the  $\sigma^+$  and  $\sigma^-$  jump points (which has also been found in Refs. 5 and 17 in the cw pump regime), the linear decay mechanism leads to the temporal delay of the jumps with respect to the pump intensity peak.

Further, we apply the developed approach to simulate the parametric scattering under pumping at the magic angle. As we show, this model allows to explain self-consistently the temporal dependences of polarizations of both the driven mode and the scattering signal which appears at the polariton branch bottom.

The paper is organized as follows. In Sec. II the available models of the multistability effect are considered and compared with each other in view of the recent experi-

mental results of Refs. 5, 17, and 19. Sec. III references the experimental setup. Sec. IV contains the experimental results and compares them with the calculations performed in the framework of the suggested model, for the cases of pumping at normal incidence (Sec. IV A) and at the magic angle (Sec. IV B), with a brief reference to some of the still unresolved issues (Sec. IV C). The results are summarized in Conclusion (Sec. V).

## II. THEORETICAL MODELS

The multistability effects in microcavities were recently considered in the framework of Gross-Pitaevskii equations written for the macro-occupied polariton modes.<sup>4,14</sup> These equations can also be written for the strongly coupled exciton and photon fields ( $\mathcal{P}$  and  $\mathcal{E}$  respectively) in the cavity active layer:<sup>16</sup>

$$i\dot{\mathcal{E}}_+ = (\omega_c - i\gamma_c)\mathcal{E}_+ + \alpha\mathcal{F}_+ + \beta\mathcal{P}_+, \quad (1)$$

$$i\dot{\mathcal{E}}_- = (\omega_c - i\gamma_c)\mathcal{E}_- + \alpha\mathcal{F}_- + \beta\mathcal{P}_-, \quad (2)$$

$$i\dot{\mathcal{P}}_+ = (\omega_x + V_1|\mathcal{P}_+|^2 + V_2|\mathcal{P}_-|^2 - i\gamma_x)\mathcal{P}_+ + A\mathcal{E}_+, \quad (3)$$

$$i\dot{\mathcal{P}}_- = (\omega_x + V_2|\mathcal{P}_+|^2 + V_1|\mathcal{P}_-|^2 - i\gamma_x)\mathcal{P}_- + A\mathcal{E}_- \quad (4)$$

(in the  $\sigma^\pm$  basis). Here,  $\mathcal{F}$  stands for the incident electric field that is usually treated as a plane wave:  $\mathcal{F}_\pm \propto e^{-i\omega_p t}$ ;  $\omega_{c,x}$  and  $\gamma_{c,x}$  are the eigenfrequencies and decay rates of the intra-cavity photon and exciton modes;  $\alpha$  and  $\beta$  are the cavity response coefficients, and  $A$  is exciton polarizability (so that  $2\sqrt{A\beta}$  equals Rabi splitting);  $V_{1,2}$  are the matrix elements of the interaction between excitons with same ( $V_1$ ) and opposite ( $V_2$ ) circular polarizations.

For simplicity, Eqs. (1–4) are written for only the driven polariton mode with zero quasi-momentum, although they can be easily generalized to the case of essentially many-mode system.<sup>16</sup> In the latter case, the usage of the exciton-photon basis (instead of the simplified polariton basis) brings the advantage of taking account of the TE/TM splitting effects as well as the angular dependence of the polariton interaction constants. As will be shown below, it is also convenient for taking account of the incoherent exciton reservoir.

The multistability conditions are defined by the relation between exciton-exciton interaction constants,  $V_1$  and  $V_2$ . According to the study of polariton spin quantum beats in a GaAs cavity,<sup>20</sup> the cross-circularly polarized excitons exhibit attraction ( $V_2 < 0$ ) that is weaker than the repulsive interaction of co-circular excitons ( $V_1 > 0$  and  $|V_2| < V_1$ ). The fact that  $V_2$  is negative is also confirmed by the rotation of polariton polarization direction during the process of parametric scattering.<sup>21</sup> In the general case the processes of exciton-exciton interaction are mediated by biexciton and dark exciton states,<sup>22–24</sup> hence the relation between the interaction constants of *polaritons* can be dependent on the exciton-photon detuning.<sup>25</sup> More precisely, one should also consider the saturation of excitonic transitions as an

additional nonlinear mechanism affecting the blueshift of polaritons under a sufficiently strong excitation.<sup>26</sup>

If  $V_1 > 0$  and  $V_2 \lesssim 0$  (as assumed in Refs. 4, 14, and 16 basing on the experimental estimations of Ref. 20), then the  $\sigma^\pm$ -components of the intra-cavity field are almost uncoupled. If  $V_2 < 0$ , then the threshold intensity  $W = |\mathcal{F}_+|^2 + |\mathcal{F}_-|^2$  of linearly polarized pump is at least two times larger than that of circularly polarized pump:  $W_{\text{thr}}^{(\text{lin})} \gtrsim 2W_{\text{thr}}^{(\text{circ})}$ .

Contrary to the above predictions,  $W_{\text{thr}}^{(\text{lin})}$  has been found to be slightly less than  $W_{\text{thr}}^{(\text{circ})}$  in the experiments using cw as well as time-resolved pumping techniques.<sup>5,17,19,27</sup> In order to explain it, two theoretical approaches have been proposed. The first one<sup>5,28</sup> presumes a repulsive interaction of polaritons with opposite pseudospins ( $\sigma^\pm$  polarizations) in the framework of Gross-Pitaevskii equations of type (1)–(4). The second approach<sup>17,29</sup> considers the additional blueshift resultant from an exciton reservoir, which leads to  $W_{\text{thr}}^{(\text{lin})} < W_{\text{thr}}^{(\text{circ})}$  without the necessity for a repulsive interaction between cross-circularly polarized excitons. (A somewhat similar model has previously been proposed in Ref. 30 to describe the interaction of a “spinless” polariton condensate with a reservoir.)

In the present work we explore the second model accounting for the transitions of the optically driven excitons into the incoherent (reservoir) state in which the overall pseudospin is relaxed, so that the reservoir provides equal blueshifts for both polarization components of the coherent state.<sup>17,29</sup> Those transitions are introduced phenomenologically as non-radiative decays of bright excitons accorded with the rate of occupation of the optically inactive reservoir. The model for the intra-cavity electric field  $\mathcal{E}$  and exciton polarization  $\mathcal{P}$  coupled with the integral population of the reservoir  $\mathcal{N}$  can be written as

$$i\dot{\mathcal{E}}_+ = (\omega_c - i\gamma_c)\mathcal{E}_+ + \alpha\mathcal{F}_+ + \beta\mathcal{P}_+, \quad (5)$$

$$i\dot{\mathcal{E}}_- = (\omega_c - i\gamma_c)\mathcal{E}_- + \alpha\mathcal{F}_- + \beta\mathcal{P}_-, \quad (6)$$

$$i\dot{\mathcal{P}}_+ = [\omega_x + V_1|\mathcal{P}_+|^2 + V_2|\mathcal{P}_-|^2 + (V_1 + V_2)\mathcal{N}/2 - i(\gamma_x + \gamma_{\text{xr}} + V_r|\mathcal{P}_-|^2)]\mathcal{P}_+ + A\mathcal{E}_+, \quad (7)$$

$$i\dot{\mathcal{P}}_- = [\omega_x + V_1|\mathcal{P}_-|^2 + V_2|\mathcal{P}_+|^2 + (V_1 + V_2)\mathcal{N}/2 - i(\gamma_x + \gamma_{\text{xr}} + V_r|\mathcal{P}_+|^2)]\mathcal{P}_- + A\mathcal{E}_-, \quad (8)$$

$$\dot{\mathcal{N}} = -\gamma_r\mathcal{N} + 2\gamma_{\text{xr}}(|\mathcal{P}_+|^2 + |\mathcal{P}_-|^2) + 4V_r|\mathcal{P}_+|^2|\mathcal{P}_-|^2. \quad (9)$$

This model is a generalization of Eqs. (1)–(4). Here,  $\gamma_{\text{xr}}$  is an additional decay rate of excitons that corresponds to the linear mechanism of light absorption, providing the term  $2\gamma_{\text{xr}}(|\mathcal{P}_+|^2 + |\mathcal{P}_-|^2)$  in Eq. (9);  $V_r$  stands for the rate of nonlinear interaction between  $\mathcal{P}_\pm$  that provides an additional occupation of the reservoir ( $4V_r|\mathcal{P}_+|^2|\mathcal{P}_-|^2$  per unit time) due to the mixture of excitons with opposite polarizations;  $\gamma_r$  stands for the reservoir own decay rate.<sup>31</sup> Microscopically, the nonlinear absorption of

cross-circularly polarized excitons is resultant from the scattering of a pair of bright excitons with opposite spins ( $J_z = -1$  and  $J_z = +1$ ) into dark excitons ( $J_z = -2$  and  $J_z = +2$ ), which is closely related to biexciton creation (see Ref. 22 for details). We do not consider the reverse transitions of incoherent (reservoir) excitons into the driven mode; this approximation is valid as long as the occupation of the reservoir states is small enough. Under resonant pumping at  $\mathbf{k} = 0$  the energy mismatch of the pump with respect to free exciton makes the filling of reservoir quite ineffective, but it is still possible due to energy level broadening and non-zero temperature. The reservoir can accumulate excitation due to its comparatively long lifetime (see Sec. IV).

Equations (5)–(9) can easily be generalized to the case of many-mode system, with exactly the same nonlinear interaction terms (which are “local” in the real space), and a linear part being in the  $k$ -space the same as in Ref. 16. In the many-mode calculations represented below in Figs. 2, 3, and 11–13, the cavity dispersion  $E_c^{\text{TE,TM}}(k)$  and response coefficients  $\alpha_{\text{TE,TM}}(k)$ ,  $\beta_{\text{TE,TM}}(k)$  for TE and TM cavity modes are properly taken into account using the transfer matrix technique.<sup>32</sup>

The two models, Eqs. (1)–(4) and (5)–(9), can give similar predictions for the cases of circular and linear polarizations of excitation. In particular, the key experimental effect waiting for explanation—that the threshold of linearly polarized pump is smaller ( $W_{\text{thr}}^{(\text{lin})} \lesssim W_{\text{thr}}^{(\text{circ})}$ )—can be reproduced within the Eqs. (1)–(4) with  $V_2 \gtrsim V_1$ . Nonetheless, the transitional dynamics under the intermediate pump polarizations  $0 < \rho_p < 1$  are completely different in the two systems, see an example in Fig. 1.

If  $V_2 < 0$  and  $V_r > 0$  (Fig. 1a, solid line, and Fig. 1b), the cavity transmission polarization increases with pump in the sub-threshold area, due to the dominant blueshift of the leading polarization component ( $\rho_p = +0.6$ ). On reaching the threshold, the leading component jumps up to the high-energy state, which causes a step-like increase in reservoir population and the blueshift of  $\sigma^-$  mode. Consequently, the minor mode also enters the above-threshold area, and the degree of circular polarization (DCP) of transmission ( $\rho_{\text{tr}}$ ) decreases down to the values smaller than the pump DCP. The same effect results in formation of the spin ring patterns under the Gaussian shaped excitation<sup>14,17,18</sup> in a close vicinity of the threshold pump power (Fig. 2). As a matter of fact, the ring shaped pattern of DCP indicates that both polarization components reach the high-energy state at the center of the pump spot where, therefore, the transmission DCP is minimal. The spatial distribution of  $\rho_{\text{tr}}$  (Fig. 2d–f) exhibits a well pronounced minimum at  $x = 0$  already when the threshold is surpassed by 1.5 times (Fig. 2e), in agreement with the experimental observations (see Fig. 3 in Ref. 17). This markedly differs from a prediction of the conventional theory based on Gross-Pitaevskii equations<sup>4,14,16</sup> with  $|V_2| \ll V_1$  (see Fig. 3) which does not exhibit the rings even at  $W/W_{\text{thr}} \approx 5$  for  $\rho_p = 0.6$ . The temporal dynamics for  $|V_2| \ll V_1$  is shown

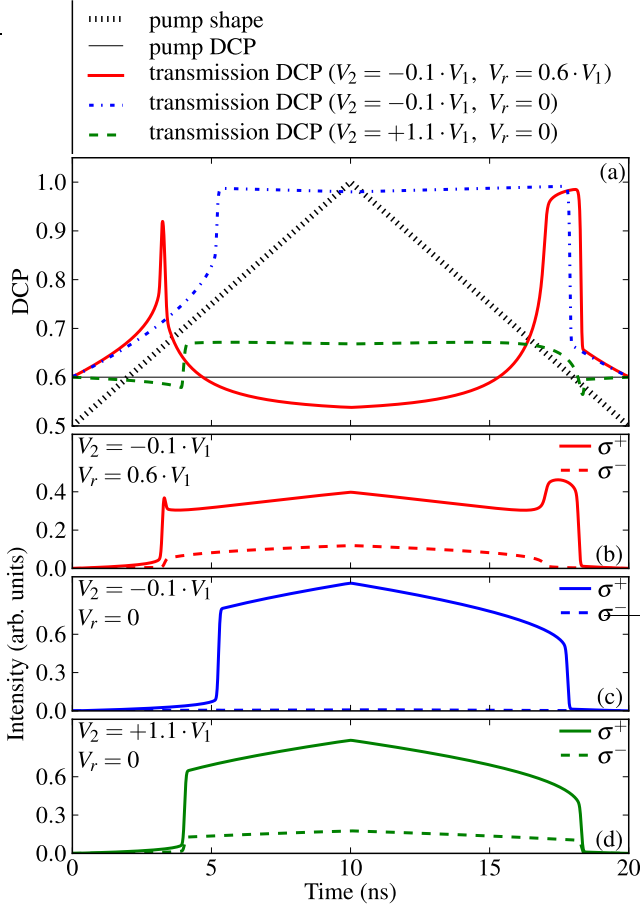


FIG. 1. (a) The calculated time dependence of the cavity transmission polarization under a slowly varying pump (transverse-dashed triangular line) with elliptical polarization. The degree of circular polarization (DCP) of pump is  $\rho_p = 0.6$  (thin solid line). Thick solid line shows the data calculated using Eqs. (5)–(9) with  $V_2/V_1 = -0.1$ ,  $V_r/(\gamma_r V_1) = 6 \text{ meV}^{-1}$ , and  $\gamma_{xr} = 0$  (explicitly as in Ref. 17). Dash-and-dot line represents the same dependence calculated using Eqs. (1)–(4) with  $V_2/V_1 = -0.1$  (this ratio was used in Refs. 4 and 14). Dash line corresponds to the case of  $V_2/V_1 = +1.1$ . The calculated data is time-averaged for each temporal point over 100 ps intervals, in order to eliminate the fast transitional effects which are not observable under the cw pump conditions. (b-d) The corresponding time dependences of the intra-cavity field intensity in  $\sigma^\pm$  polarization components.

in Fig. 1a (dash-and-dot line) and in Fig. 1c.

In the opposite case, when  $V_2 > V_1$  and the system is “purely coherent” (Fig. 1a, dash line, and Fig. 1d), which also corresponds to the right relation  $W_{\text{thr}}^{(\text{lin})} < W_{\text{thr}}^{(\text{circ})}$ , the polarization dynamics is completely different. First, the transmission DCP decreases in the sub-threshold area, since an increase in the “leading”  $\sigma^+$  component provides a larger blueshift for  $\sigma^-$ , so that the difference in  $\sigma^\pm$  intensities weakens with increasing pump. On reaching the threshold,  $\rho_{\text{tr}}$  shows a minor step-like increase followed by the very weak changes with further increasing

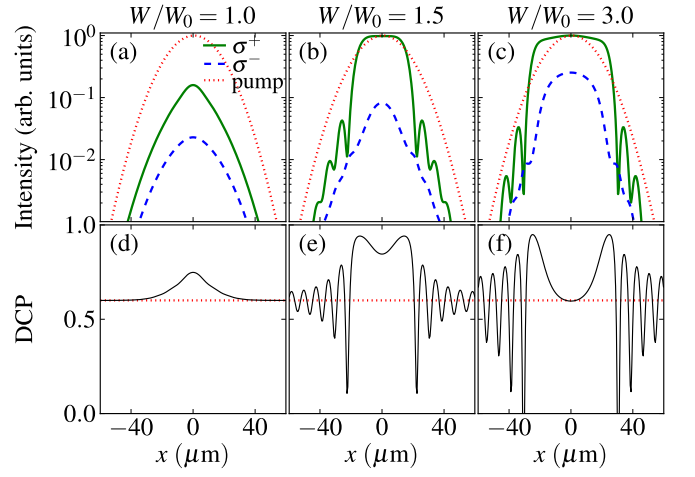


FIG. 2. The calculated “spin ring” pattern formation in the framework of many-mode model Eqs. (5)–(9) with  $V_r = 0.6 \cdot V_1$ ,  $V_2 = -0.1 \cdot V_1$ , and  $\gamma_{xr} = 0$  (explicitly as in Ref. 17). The pump DCP is  $+0.6$  (as in Fig. 1). Panels a–c show the spatial distribution of intensity of the intra-cavity field in  $\sigma^+$  and  $\sigma^-$  polarization components (solid and dashed lines, respectively), for several values of pump power  $W$ ; the pump distribution profile is shown by dotted lines.  $W_0$  roughly corresponds to the threshold excitation density. Panels d–f represent the corresponding spatial distribution of the intra-cavity field DCP.

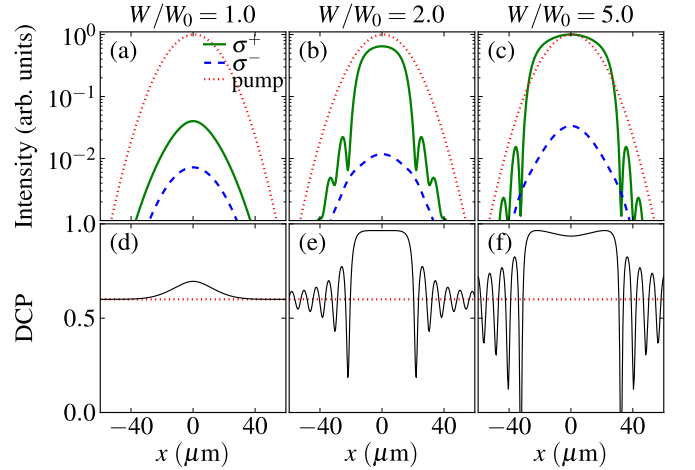


FIG. 3. The calculated spatial distribution of the intra-cavity field for  $V_r = \gamma_{xr} = 0$  and  $V_2 = -0.1 \cdot V_1$ . All other parameters coincide with those of Fig. 2. Unlike Fig. 2, almost no ring structure appears in the cavity transmission DCP even at  $W/W_0 = 5$ .

pump power. No prerequisites for the spin ring formation are satisfied in this case.

Thus, the observed phenomena—the disparity of thresholds,  $W_{\text{thr}}^{(\text{lin})} \lesssim W_{\text{thr}}^{(\text{circ})}$ , together with the field polarization dynamics—cannot be reproduced within Eqs. (1)–(4) using only two constants  $V_{1,2}$  of exciton-exciton interaction even if a single polariton mode at  $\mathbf{k} = 0$  is considered. The experiments revealing both

the energy (blueshift) and polarization dynamics of the driven polariton mode under the nanosecond-long excitation pulses are described below in Sec. IV.

### III. EXPERIMENT

The microcavity structure grown by a metal-organic vapor-phase epitaxy technique has top (bottom) Bragg reflectors composed of 17 (20)  $\lambda/4$   $\text{Al}_{0.13}\text{Ga}_{0.87}\text{As}/\text{AlAs}$  layers. The  $3\lambda/2$  GaAs cavity contains six 10 nm thick  $\text{In}_{0.06}\text{Ga}_{0.94}\text{As}/\text{GaAs}$  quantum wells. The Rabi splitting is about 6 meV. A gradual variation of the active layer thickness along the sample provides a change in the photon mode energy  $E_c = \hbar\omega_c$  and, accordingly, in the detuning  $\Delta$  between the exciton  $E_x(k=0)$  and photon  $E_c(k=0)$  mode energies. Experiments are carried out in several regions of the same sample with  $\Delta \approx 0$  (Sec. IV A) and  $\Delta \approx -1.5$  meV (Sec. IV B).

The sample is placed into the optical cryostat with controlled temperature. To excite the cavity, we use a pulsed Ti:sapphire laser producing picosecond long pulses at a repetition rate of 5 kHz. Prior to coming into the cryostat, the pulses pass through a long multi-mode optical fiber and then through a monochromator. After the fiber, the pulses have a duration of about 1 ns, and after the monochromator they have spectral full width at half maximum (FWHM) of 0.7 meV. The excitation is performed either along the normal to the cavity plane ( $k_p = 0$ ) or at the magic angle ( $k_p = 1.8 \mu\text{m}^{-1}$ ) slightly above the lower polariton branch resonance, with various pump polarizations (circular, linear, or elliptical). The main axis of pump polarization is directed along the  $\langle 110 \rangle$  axis of the structure. The pump beam is focused onto the spot with a diameter of  $100 \mu\text{m}$ . The kinetics of the cavity transmission signal  $I_{\text{tr}}(t)$  is detected at  $T \approx 6$  K by the streak camera with spectral, angular, and time resolution of 0.28 meV,  $0.5^\circ$ , and 70 ps, respectively, in various polarizations. The temporal dependences of the signal are averaged over  $\sim 10^4$  pulses, for we have to collect the signal in order to eliminate noises.

## IV. EXPERIMENTAL RESULTS AND DISCUSSION

### A. Pumping at normal incidence ( $k_p = 0$ )

The information on the intra-cavity field kinetics is obtained from the cavity transmission measurements.<sup>12,33</sup> The active region of the cavity is separated from a detector by the Bragg mirror that does not introduce any nonlinearity and/or spectral selectivity. Thus, the intensity of the transmission signal,  $I_{\text{tr}}(\omega, t)$ , is proportional to the squared magnitude of the intra-cavity electric field  $|\mathcal{E}(\mathbf{k}_p, \omega, t)|^2$ , and the first momentum  $\bar{E} = \hbar \int \omega I_{\text{tr}}(\omega, t) d\omega / \int I_{\text{tr}}(\omega, t) d\omega$  at  $\mathbf{k} = \mathbf{k}_p$  reflects the time

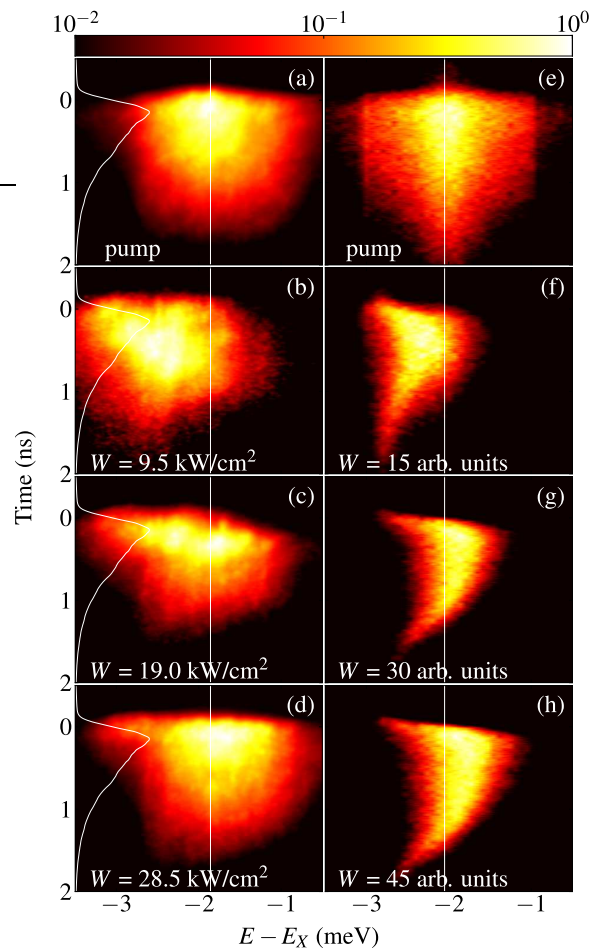


FIG. 4. Time and energy dependences of the excitation pulse (a, e) and cavity transmission intensity  $I_{\text{tr}} = I_{\text{tr}}(E, t)$  for different pump powers  $W$  (b–d and f–h). The pump is polarized circularly. The normalized temporal shape of the excitation is shown at the left side (white solid line); the weighted mean value of the pump energy is shown by the vertical line. Left and right panels represent the experimental and calculated data, respectively. The color scale is logarithmic.

dependence of the average (effective) energy of excited mode  $\bar{E}(t)$ .

Figures 4b–d show the measured time dependences of transmission signal  $I_{\text{tr}}(t)$  under the excitation with circularly polarized ( $\sigma^+$ ) light. The spectra are recorded in the same  $\sigma^+$  polarization; the fraction of signal in the opposite polarization ( $\sigma^-$ ) does not exceed a few percent. At low peak excitation density  $W \equiv \max_t I_{\text{tr}}(t) \approx 9.5 \text{ kW/cm}^2$  the maximum of the signal is found at the low energy side of the excitation, near the lower polariton eigenfrequency. Although the blueshift in polariton energy remains relatively small, the time dependence of the signal differs markedly from that of the pump pulse. This indicates the onset of nonlinear processes at the red edge of pump spectrum. In particular, the maximum of the signal is delayed for a few hundred picoseconds with respect to the pump peak. Nonlinearities in both the

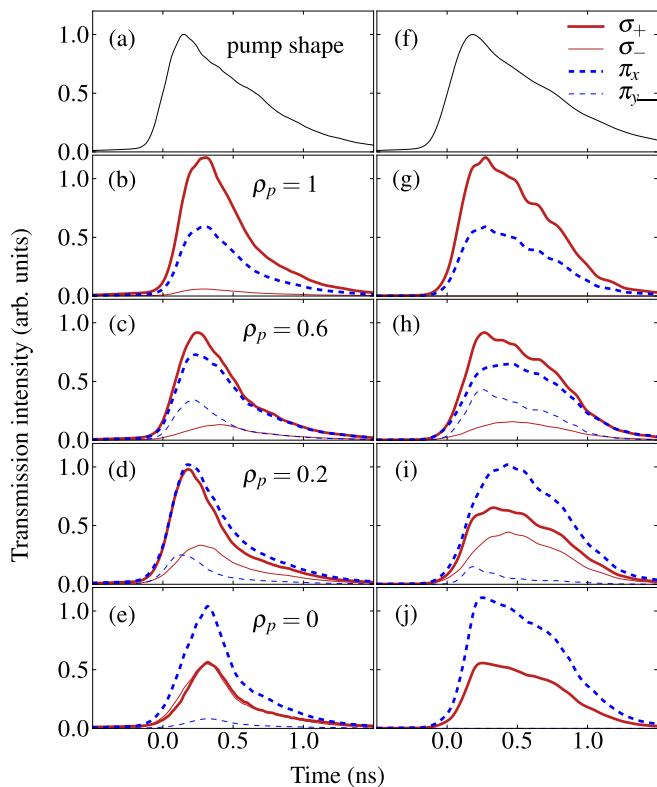


FIG. 5. Time dependences of the cavity transmission intensity, in circular and linear polarization components ( $\sigma^\pm$  and  $\pi_{x,y}$ , resp.) for different pump polarizations  $\rho_p$  (circular, elliptical, and linear polarizations). The top panels show the time shape of the exciting pulse. Left and right panels represent the experimental and calculated data, respectively. In the experiment,  $W = 28.5 \text{ kW/cm}^2$ .

magnitude and spectral position of the signal increase with pump power: as the peak energy of the signal shifts up to the pump energy  $E_p$ , (i) the signal intensity shows the superlinear (threshold like) increase and (ii) the time when the signal reaches its maximum value shifts backward to the onset of excitation pulse.

The observed correlation between the energy blueshift and intensity of the signal is expected in the framework of the multistability model<sup>4</sup> Eqs. (1)–(4), however this model fails to explain the process of instability development. Figures 4e–h show that the observed time and spectral dependences can be qualitatively reproduced in simulations using Eqs. (5)–(9) with appropriate time and energy shapes of the excitation (see Appendix). The chosen parameters of microcavity coincide with those used in the experiment; the constants of interaction with reservoir are considered below.

The temporal dependence of transmission under the excitation with linearly, elliptically and circularly polarized pulses (DCPs 0, 0.2, 0.6, and 1) at  $W = 28.5 \text{ kW/cm}^2$  is shown in Fig. 5. The temporal delay of the dominating  $\sigma^+$  and  $\pi_x$  polarization components of the signal with respect to the pump peak is seen to be

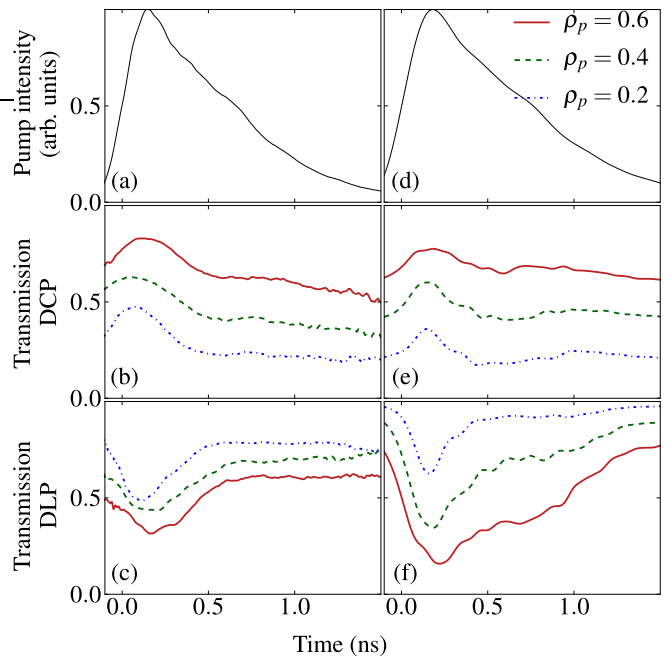


FIG. 6. Time dependences of degrees of circular (b, e) and linear (c, f) polarizations of the transmitted pulses, for several values of the pump DCP ( $\rho_p = 0.2, 0.4, 0.6$ ). Left and right panels represent experimental and calculated data, respectively. In the experiment,  $W = 28.5 \text{ kW/cm}^2$ .

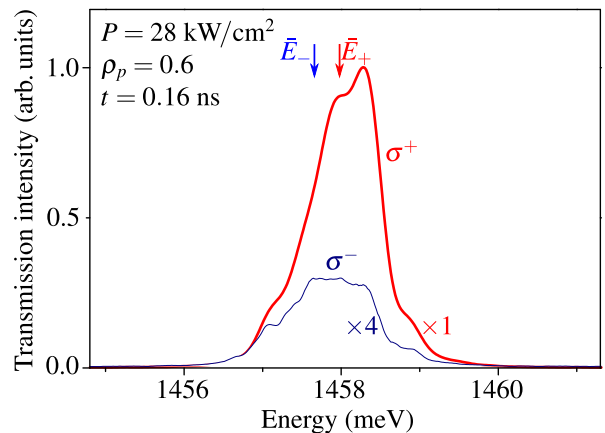


FIG. 7. The spectrum of intra-cavity field in  $\sigma^\pm$  components in the range of polarization instability (experiment). Weighted mean values of the energy  $\bar{E}_\pm$  are indicated by arrows.

in the range of 150–200 ps, which is much larger than the lifetime of polaritons with  $k = 0$ . The “anomalous” increase in the intra-cavity field observed in the range of decreasing pump power (after the pump peak is already passed) can be explained by the blueshift in effective polariton energy. In turn, this blueshift could only be provided by the long-lived polariton states accumulated during the pulse. Such an effect corresponds to the “linear” process of polariton scattering into the exciton

reservoir, which is determined by the ratio between  $\gamma_r$  and  $\gamma_{xr}$  in Eqs. (7)–(9). The experimental results are qualitatively reproduced in numerical simulations with  $V_2/V_1 = -0.1$ ,  $V_r/V_1 = 7 \cdot 10^{-3}$ ,  $\hbar\gamma_r = 2 \cdot 10^{-3}$  meV, and  $\gamma_{xr} = 3 \cdot 10^{-3}$  meV. These parameters are chosen to meet the following conditions: (i) the overall occupation of the reservoir is comparable to that of the driven (optically active) polariton mode, so that  $W_{\text{thr}}^{(\text{lin})} \lesssim W_{\text{thr}}^{(\text{circ})}$ , and (ii) the temporal peak of the signal can be delayed by hundreds of picoseconds with respect to the excitation peak even for  $\rho_p = \pm 1$ . Note the long decay times of the reservoir states,  $\sim 300$  ps. So long times are characteristic of excitons localized due to fluctuations of quantum well potential and/or free excitons with large lateral wave numbers.

Figures 5b and 5e reveal the transmission signal to be retaining both circular and linear pump polarizations; in these cases only a weak depolarization of the transmitted light is observed. Retaining of the circular polarization in agreement with the angular momentum conservation law is expected. Measurements performed under linearly polarized pump in a wide range of  $W = 9.5 - 28.5$  kW/cm<sup>2</sup> (not shown) have revealed the magnitude of transmitted light depolarization to be within the limits of 12–17%, almost independently of the pump power. On the other hand, under the elliptically polarized excitation ( $0 < \rho_p < 1$ ) the signal DCP does depend on the pump intensity due to the anisotropy in polariton-polariton interaction.<sup>4</sup> Accordingly, the ratio between both circularly and linearly polarized components of the signal intensity ( $\sigma^\pm$  and  $\pi_{x,y}$ , respectively) varies with time (Fig. 5c,d). The corresponding temporal dependences of the degrees of circular and linear polarizations of the signal are shown in Fig. 6. From comparison of Figs. 5 and 6, it is seen that the reaching of maximum signal intensity at  $t \approx 0.2$  ns is accompanied by a decrease in the signal DCP, in much the same way as the cw driven system behaves (Fig. 1), though the latter system exhibits the expectedly sharper transitions. On the other hand, our experimental technique allows us to visualize the energies of intra-cavity field in addition to their intensities. The information on the energies is extracted from the transmission spectra as shown in Fig. 7 since  $I_{\text{tr}}(\hbar\omega) \propto |\mathcal{E}(\hbar\omega)|^2$ . The energies of intra-cavity field in  $\sigma^+$  and  $\sigma^-$  polarizations demonstrate a well pronounced blueshift with increasing polariton density and a well pronounced splitting. In particular it is seen in Fig. 7 that in the range of maximum polarization the  $\sigma^+$  component of the field is markedly (by 0.3 meV) blue-shifted with respect to  $\sigma^-$ .

The basis in which shown degree of linear polarization (DLP) was measured is related to the pump polarization axis. We observe no linear polarization in the basis rotated by 45° with respect to the former one. Thus, the sum of squared Stokes parameters per signal intensity is less than 1, which means that the signal is partially depolarized; this is because the signal polarization components are measured as averaged quantities.

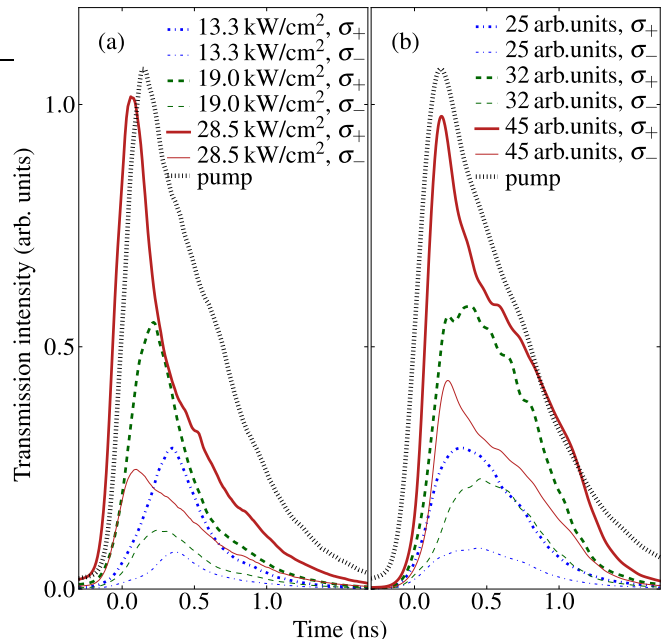


FIG. 8. Time dependences of the transmission DCPs, for several values of the pump power  $W$ , under excitation with elliptically polarized pulses with  $\rho_p = 0.4$ . Grey dotted line corresponds to the normalized temporal shape of excitation. Left and right panels represent experimental and calculated data, respectively.

In order to clarify the physics underlying the signal polarization transitions, let us consider the series of measurements performed under elliptically polarized pulses with  $\rho_p = 0.4$  and various pump intensities. Fig. 8 represents measured (left side) and calculated (right side) time dependences of the transmission signal in  $\sigma^\pm$  polarization components. From these series, the pump power dependence of the temporal delay between the signal and pump peaks is evidenced. The certain conditions for a switch in signal polarization depend on both the pump intensity and its temporal shape. In case of the very low pump densities, the intra-cavity field is insufficient for multistability to reveal; on the other hand, if the pump density is increasing quickly enough then a jump into a high-energy state happens with no delay related to the long-lived reservoir, since most of the intra-cavity field is concentrated in the driven (optically active) polariton state. Except the case of maximum  $W$ , the dynamics shown in Fig. 8 lies in the intermediate range of pump powers which all are insufficient to pull a polariton state by itself up to the threshold magnitude. Instead of that, the non-equilibrium transitions proceed through the mediation of excitation accumulated by the reservoir. In such a case the development of instability in the leading polarization component ( $\sigma^+$ ) always precedes the reservoir induced switch in signal polarization.

Figure 9, which also shows a series for two peak pump intensities at fixed  $\rho_p = 0.4$ , allows us to visualize the

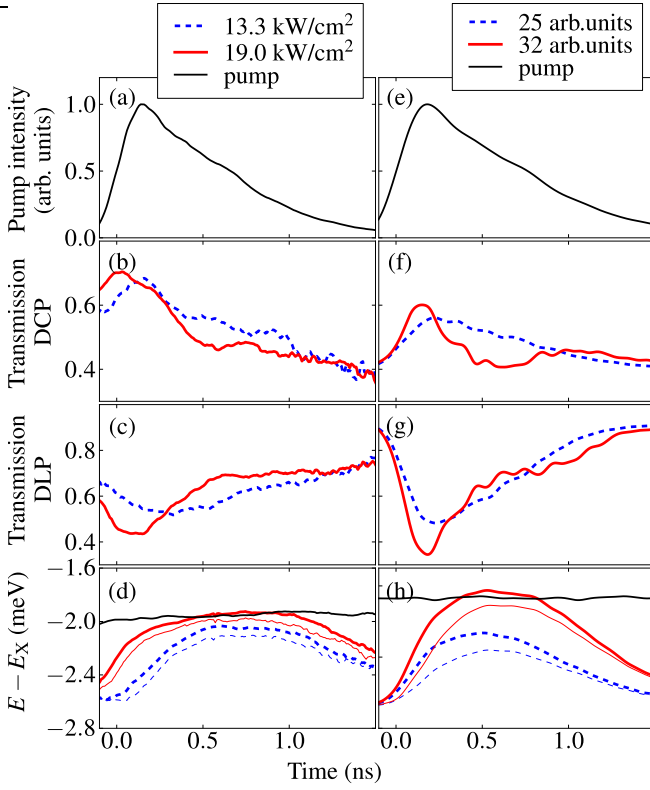


FIG. 9. Time dependences of the pump pulse intensity (a, e), degrees of circular (b, f) and linear (c, g) polarizations (DCP and DLP) of the transmitted pulse, and the weighted mean values  $\bar{E}_\pm$  of the transmission energy in  $\sigma^+$  (thick lines) and  $\sigma^-$  (thin lines) polarization components (d, h), for several values of the pump power  $W$ . The pump DCP is 0.4. The mean value of pump energy, which exhibits minor variations in a close vicinity of  $E - E_x = -2$  meV, is shown by solid thin lines in panels (d, h). Left and right panels represent experimental and calculated data, respectively.

temporal correlations between the energy (in both  $\sigma^\pm$  polarization components) and polarization degree of the transmission signal. The overall process of the instability development is accompanied by blueshifts in  $\sigma^\pm$  energies. At the first stage (which starts the earlier, the higher is pump density  $W$ ), the leading polarization component ( $\sigma^+$ ) enters the region of positive feedback between its effective resonance energy  $\bar{E}_+$  and the  $\sigma^+$  field amplitude, so the difference in  $\sigma^\pm$  energies grows along with the DCP of transmission signal (Fig. 9b, d). Accordingly, a well pronounced decrease in the DLP of transmission is observed at the same time interval (Fig. 9c). At approximately the half way through the energy growth (see panel d), the integral occupation of reservoir becomes sufficient to provide the shift in the minor component ( $\sigma^-$ ), which leads to decrease in both the energy difference  $\bar{E}_+ - \bar{E}_-$  and DCP, and to the corresponding increase in DLP. All these effects are qualitatively reproduced in calculations shown in Fig. 9e-h. Thus, the observed dynamics confirm the effect of reser-

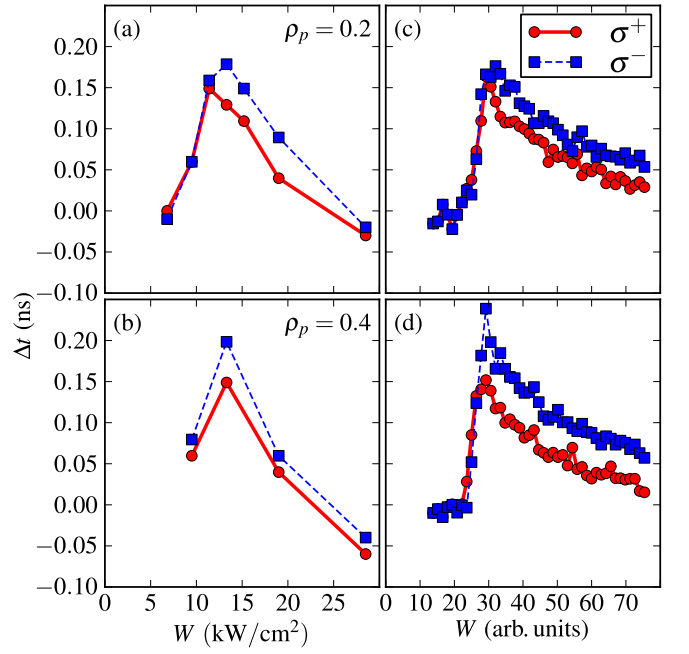


FIG. 10. The effective delay of the  $\sigma^\pm$  components of the signal with respect to the pump vs. pump power (as defined by Eq. (10)), for two pump polarizations,  $\rho_p = 0.2$  (panels a, c) and  $\rho_p = 0.4$  (panels b, d). Left and right sides of the figure represent experimental and calculated data, respectively.

voir, though the energy broadening makes the transitions much smoother compared to the cw driven system (Fig. 1).

Figure 10 shows the time delay of the signal with respect to the excitation pulse in a wider range of pump powers  $W$ ; it summarizes the consideration of the threshold effects in the cavity transmission. The value of the delay  $\Delta t$  is determined as the difference between the moments the signal and the pump reach their half-maxima for the first time:

$$\Delta t_\pm = t \Big|_{I_{tr}^\pm(t) \rightarrow \frac{1}{2} \max_t I_{tr}^\pm(t)} - t \Big|_{I_p(t) \rightarrow \frac{1}{2} \max_t I_p(t)}. \quad (10)$$

At small  $W$  the response is linear, and the delays  $\Delta t$  are expectedly small. At threshold, the superlinear growth of the signal is observed with  $\Delta t$  of about 150 to 200 picoseconds, i.e. at the back front of excitation. Thus, this transition is induced by the reservoir as explained above. With further increasing  $W$ , the optically active fraction of excitons grows, which lowers the system's inertness, and the delay of response decreases. Note, that the minor ( $\sigma^-$ ) polarization component exhibits the superlinear growth at the same *peak* power  $W$  as  $\sigma^+$ , and the relative delay of  $\sigma^+$  and  $\sigma^-$  components,  $\Delta t_+ - \Delta t_-$ , remains nearly constant above the threshold. This is an extra evidence of the fact that the jump in the minor component is provided by the reservoir even at high  $W$ .

## B. Pumping at the magic angle ( $k_p = 1.8 \mu\text{m}^{-1}$ )

Let us now consider the polarization properties of the signal of parametric scattering—generally referred to as cavity “optic parametric oscillator” (OPO) signal<sup>2</sup>—which appears at the branch bottom ( $k = 0$ ) if pumping is at the magic angle ( $k_p \approx 1.8 \mu\text{m}^{-1}$ ). There are two points to discuss here. First, in the general case of elliptically polarized excitation the signal is expected to reflect variations in the DCP of the driven mode that, in turn, are shown to be strongly affected by the excitonic reservoir. Second, if the pump is polarized linearly, the experiments show the  $90^\circ$  rotation of the signal polarization axis;<sup>21</sup> thus, we have to check if Eqs. (5)–(9) can reproduce this effect in spite of the reservoir induced interaction between the cross-circularly polarized excitons.

The experiments are carried out at negative detuning between the photon and exciton ( $\Delta \approx -1.5 \text{ meV}$ ) in order to have the pump frequency close to that employed for the normal incidence pumping considered in Sec IV A. The cavity and excitation parameters used in the simulations coincide with the experimental ones, whereas the nonlinear interaction constants as well as reservoir characteristics are the same as used in the previous Section.

Figure 11 represents measured and calculated dynamics of intra-cavity field at  $k = k_p$  (which corresponds to the cavity transmission) and  $k = 0$  (OPO signal) under elliptically polarized excitation with DCP = 0.5 and different pump powers  $W$ . When  $W$  exceeds the critical value (in the experiment  $W_{\text{thr}} \approx 10 \text{ kW/cm}^2$ ), a well pronounced superlinear growth of the cavity transmission (Fig. 11b) is observed at  $t = 0.1 - 0.4 \text{ ns}$ . Near the threshold, a doubling of the pump power  $W$  leads to an order-of-magnitude growth of the OPO signal intensity (Fig. 11e). The observed nonlinearities indicate the onset of parametric instability, being, however, by far not as sharp as under cw excitation.<sup>11</sup>

The dynamics of the driven mode is similar to that under the pumping at normal incidence. The growth of the field amplitude, which continues with increasing pump density (Fig. 11b), expectedly leads to the growth of transmission DCP (Fig. 11c) due to the dominantly repulsive exciton-exciton interaction. At  $t = 0.1 - 0.4 \text{ ns}$  the transmission starts to behave strongly nonlinearly with respect to the driving field, and the peak of transmission becomes significantly delayed with respect to the peak of pump pulse. The latter indicates that the transition is assisted by the reservoir induced blueshift. Accordingly, the jump in transmission DCP is immediately followed by dropping back as soon as the system enters the above-threshold region where the energies of  $\sigma^\pm$  components of intra-cavity field (Fig. 11d) become partially levelled due to the reservoir filling.

The domination of the leading polarization component ( $\sigma^+$ ) is strongly enhanced in the OPO signal (Fig. 11f) whose DCP reaches 0.85 at  $t \approx 0.2 \text{ ns}$ . The subsequent lowering of DCP of the driven mode forces the OPO signal, too, to partially loss its polarization. However, the

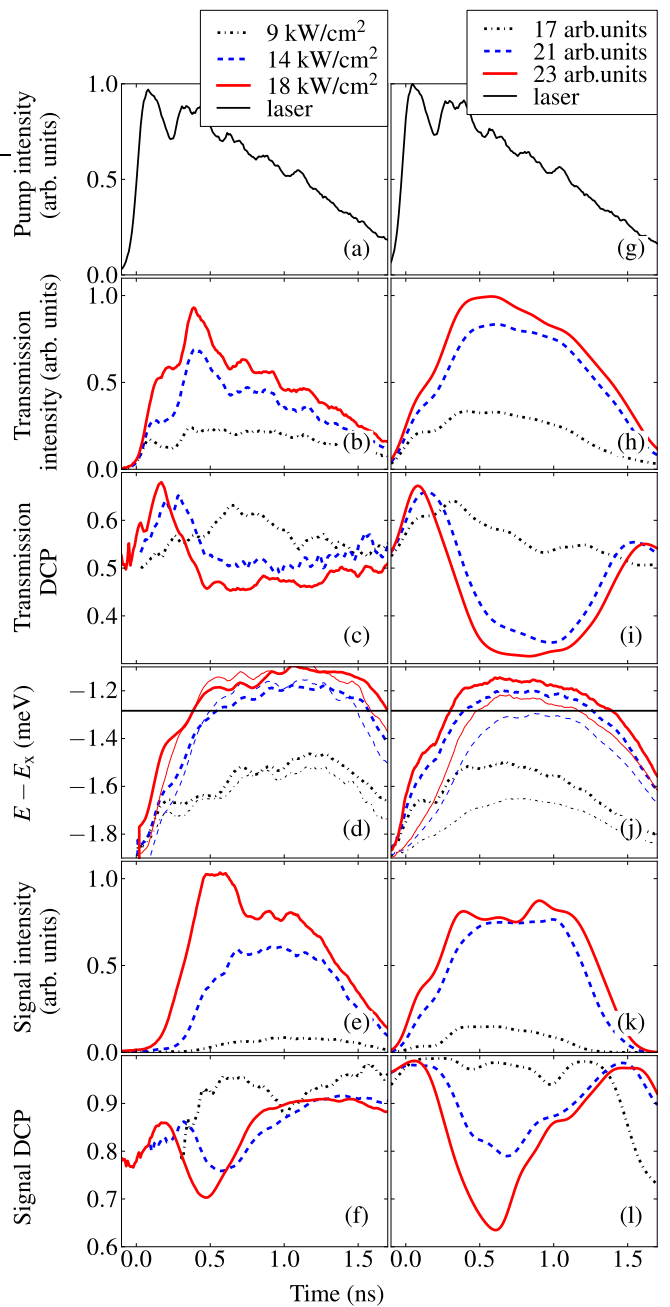


FIG. 11. Time dependences of the pump pulse intensity (a, g), transmission intensity (b, h), transmission DCP (c, i), weighted mean values of the transmission energy  $\bar{E}_\pm$  (d, j) in two polarization components  $\sigma^+$  and  $\sigma^-$  (thick and thin lines, resp.), OPO signal intensity (e, k) and DCP (f, l), for several values of the pump power  $W$ . Straight lines in panels c, i indicate the mean value of pump energy. Left and right panels represent experimental and calculated data, respectively.

signal restores a high DCP during the further evolution accompanied by the decrease in transmission intensity. The calculations performed on the basis of Eqs. (5)–(9), which are presented in the right panels of Fig. 11, reproduce the observed threshold-like behavior of intra-cavity

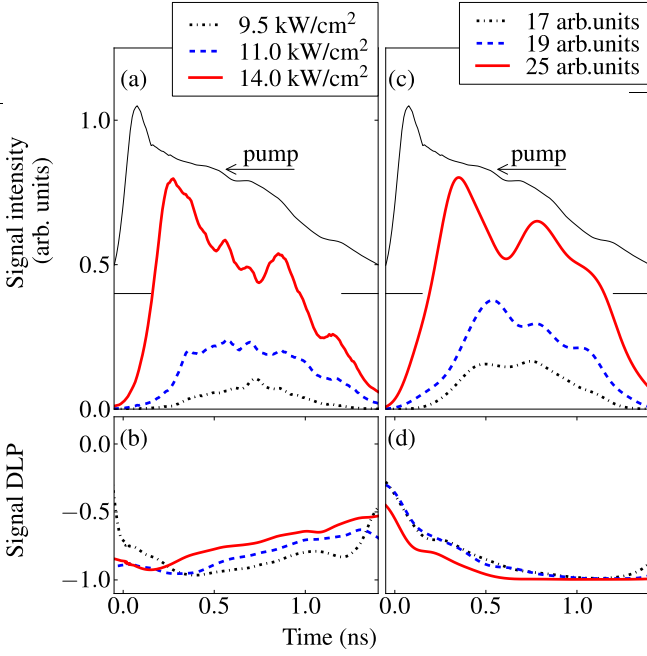


FIG. 12. Time dependences of the OPO signal intensity (*a*, *c*) and degree of linear polarization (*b*, *d*) under the pump  $\vec{F}(t)$  polarized linearly along the TM cavity mode ( $\vec{F} \parallel \vec{E}_{\text{TM}}$ ), for some different values of the pump power  $W$ . Left and right panels represent the experimental and calculated data, respectively. The temporal shape of excitation is indicated in panels *a*, *c* as a guide for eye.

field along with its polarization properties. However, a quantitative agreement is not achieved, partially due to a complicated spectral shape of the pump pulses (see Fig. 4) and due to intrinsic limitations of the suggested theoretical model (see discussion in Sec. IV C).

Let us turn to the case of exactly linear polarization of the excitation at  $k_p > 0$  (Figs. 12 and 13). In this case the OPO signal depends on whether the pump excites a pure cavity state—one of TE and TM modes which are the eigenstates of 2D photon in the empty cavity—or a mixture of both the TE and TM components. Fig. 12 represents the dynamics of OPO signal under the pump polarized along the TM cavity mode. In the range of high intensity of the signal, its degree of linear polarization (DLP) reaches 90%. The polarization axis is  $90^\circ$  rotated with respect to the pump (what corresponds to negative DLP values), which is well reproduced in the calculations.

On the other hand, if the pump is polarized in between the TE and TM directions ( $\vec{F} \parallel [\vec{E}_{\text{TE}} + \vec{E}_{\text{TM}}]$ , Fig. 13), the signal DLP does not exceed 30% in the range of a strong signal (Fig. 13*e*). The shown DLP values were measured (and calculated) in the basis of directions parallel and orthogonal to pump polarization; there is no marked DLP in the TE-TM basis as well. This effect is explained by the lifted degeneracy (TE-TM splitting) of cavity modes which leads to the variation with time of the  $\sigma^\pm$  phase shift. Accordingly, it causes the misbalance of  $\sigma^+$  and  $\sigma^-$

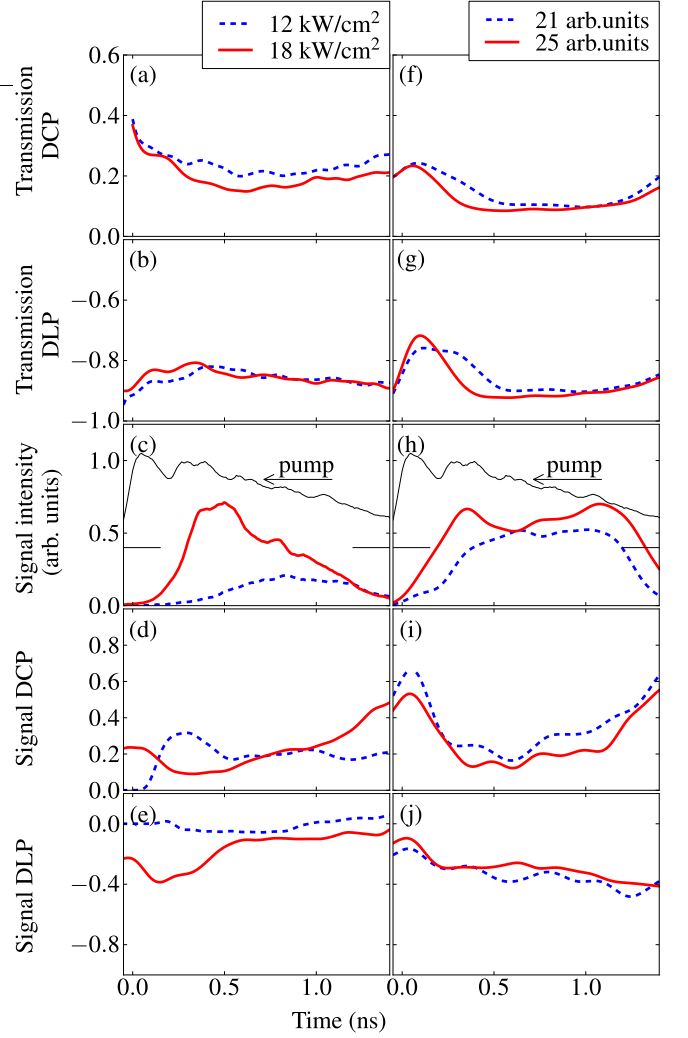


FIG. 13. Time dependences of the transmission DCP (*a*, *f*), transmission DLP (*b*, *g*), signal intensity (*c*, *h*), signal DCP (*d*, *i*), and signal DLP (*e*, *j*) under linearly polarized pump wave  $\vec{F} \parallel (\vec{E}_{\text{TE}} + \vec{E}_{\text{TM}})$ . Left and right panels represent experimental and calculated data, respectively. The temporal shapes of excitation are indicated in panels *a*, *c* as a guide for eye. In calculation, the TE/TM splitting of the driven polariton mode equals to 0.06 meV.

components of intra-cavity field, i. e. a reduced DLP and non-zero DCP of the driven mode (Fig. 13*a*, *b*), which is seen in both measured and calculated data. Due to permanent modification of the direction of signal polarization, the eventual OPO signal appears to be significantly depolarized (the sum of squared DCP and DLP is markedly less than 1, Fig. 13*d*, *e*).

Thus, the dynamics of the OPO signal confirms the effect of reservoir. Under elliptic excitation, the  $\sigma^\pm$  polarization components tend to be levelled by the reservoir. By itself, this effect could be assigned to a repulsion between cross-circularly polarized excitons ( $V_2 > 0$ ). On the other hand, the axis of signal polarization is found in-

verted with respect to the pump, which restricts the sign of  $V_2$  to be negative irrespectively of the reservoir induced blueshifts. Since we have reproduced these effects within Eqs. (5)–(9), it is proven to provide a self-consistent description of the intra-cavity field polarization dynamics.

### C. Shortcomings

We have shown that the semi-phenomenological Eqs. (5)–(9) explain the observed polarization dynamics in a good qualitative agreement with the experimental data. Let us now consider the limitations of the suggested approach. Its most important shortcoming is the absence of a feedback between the driven polariton modes and the exciton reservoir, as long as the latter is introduced using the integral occupation number  $\mathcal{N}$ , neglecting the actual microscopic distribution of reservoir states. As a result, Eqs. (5)–(9) do not describe, e. g. the establishing of equilibrium between coherent and incoherent exciton “phases” which would normally take place in a real system; this process implies (i) the reverse transitions from the reservoir into the macro-occupied mode (similar to Bose-Einstein condensation) and (ii) dependence of the scattering rates ( $\gamma_{xr}$  and  $V_r$ ) on the polariton density. These shortcomings lead to several visible discrepancies between the measured and calculated data. In particular, the superlinear drop in transmission intensity observed at the back front of exciting pulses, which is evident from comparison of left and right panels of Fig. 8, is not reproduced by the present model. Note as well that the nonlinear scattering rate  $V_r$  should depend on the energy of biexciton resonance which mediates the transitions of optically driven polaritons into the reservoir.<sup>23,24</sup> Accordingly, the actual relation between the multistability thresholds  $W_{\text{thr}}^{(\text{circ})}$  and  $W_{\text{thr}}^{(\text{lin})}$  would depend on the pump frequency as well as on the frequency detuning between photon and exciton modes.

As a result, we expect Eqs. (5)–(9) to be qualitatively valid in the case of resonant excitation of the optically active cavity states. On the other hand, in the cases of comparably large pump wave numbers and/or non-resonant excitation conditions, when a much larger contribution of reservoir excitons is expected, the model is likely to become unsatisfactory.

## V. CONCLUSION

In the present work we have studied the non-equilibrium transitions in a multistable system of cavity polaritons under resonant nanosecond-long excitation. Using the spectrally broadened pulses, we have visualized the temporal correlations between the effective resonant energy, intensity, and optical polarization of the intra-cavity field which all undergo the strong changes on reaching the threshold pump power. In the vicinity of

the threshold, the dynamics of such system is strongly affected by the long-lived exciton reservoir (excited due to polariton scattering) which influences both the characteristic times of instability development and output signal polarization.

The temporal behavior of the intra-cavity field is found to be not described in the conventional model based on the Gross-Pitaevskii equations written for purely coherent macro-occupied polariton states. Most importantly, the observed phenomena cannot be explained even qualitatively within a model with only the two exciton-exciton interaction constants ( $V_{1,2}$ ) allowed for. To explain the experiments, we have proposed the model for the macro-occupied polariton states coupled with an exciton reservoir. In spite of some limitations, this model provides a self-consistent description of the observed intra-cavity field dynamics under both pulse and continuous wave excitation conditions.

Authors thank M. S. Skolnick for rendered samples, D. N. Krizhanovskii for fruitful discussions, and A. V. Larionov for assistance in the experiment. This work was supported by Russian Foundation for Basic Research and the Russian Academy of Sciences.

### Appendix: Details on numeric modeling

In attempt to reproduce the experimental pump spectrum, which is characterized by FWHM of about 0.8 meV and, hence, has a lowered coherence, the modeled pump is ‘broadened’ by means of the partial randomization of phases of different spectral harmonics. Namely, the pump amplitude is defined as follows:

$$\mathcal{F}_{\pm}(t) = \mathcal{F}_{\pm}^{(0)}(t) \left( \frac{\mathcal{R}(t)}{|\mathcal{R}(t)|} \right) \exp(-i\omega_p t - i\varphi_{\pm}); \quad (\text{A.1})$$

$$\mathcal{R}(t) = \sum_{n=1}^N \exp\left(-\frac{\omega_n^2}{2\sigma^2} - i\omega_n t - \frac{2i\pi}{N} \sum_{m=1}^n \chi_m\right). \quad (\text{A.2})$$

Here,

- $\mathcal{F}_{\pm}^{(0)}(t)$  are real-valued amplitudes of the  $\sigma^{\pm}$  polarization components;
- $\varphi_+ - \varphi_-$  defines the direction of the polarization axis;
- $\omega_p$  is the central pump frequency;
- $\omega_n = \Omega \left( \frac{n}{N} - \frac{1}{2} \right)$ ,  $n = 1, 2, \dots, N$ ;  $N = 1000$ ;  $\Omega = 2 \text{ meV}$ ;
- $\sigma = \text{FWHM} / \sqrt{8 \log 2}$  defines the width of the pump spectrum,  $\text{FWHM} = 0.8 \text{ meV}$ ;
- $\{\chi_m \mid m = 1, 2, \dots, N\}$  is a set of random uniformly distributed numbers within the interval  $[0; 1)$ .

The spectral FWHM of the pump defined such a way approximately coincides with experimental one, and its coherence time is about 5 picoseconds. Under these conditions the system is inevitably stochastic. Hence, for each set of parameters Eqs. (5)–(9) are solved a number of times (20–100) with different  $\{\chi\}$  until the averaged evolution of the signal intensity becomes independent on

the number of realizations. This corresponds to the collection of numerous signals, which allows us to reduce noises. The degrees of polarization are then calculated using the *averaged* intensities. As a result, the transmission can be partially depolarized (under elliptically polarized excitation) due to small random differences in the individual pulses in much the same way as the measured signal.

- 
- \* gavr'ss@issp.ac.ru
- <sup>1</sup> C. Weisbuch, M. Nishioka, A. Ishikawa, and Y. Arakawa, *Phys. Rev. Lett.* **69**, 3314 (1992).
  - <sup>2</sup> A. V. Kavokin and G. Malpuech, *Cavity Polaritons* (Elsevier, Amsterdam, 2003).
  - <sup>3</sup> A. Baas, J. P. Karr, H. Eleuch, and E. Giacobino, *Phys. Rev. A* **69**, 023809 (2004).
  - <sup>4</sup> N. A. Gippius, I. A. Shelykh, D. D. Solnyshkov, S. S. Gavrilov, Y. G. Rubo, A. V. Kavokin, S. G. Tikhodeev, and G. Malpuech, *Phys. Rev. Lett.* **98**, 236401 (2007).
  - <sup>5</sup> T. K. Paraíso, M. Wouters, Y. Léger, F. Morier-Genoud, and B. Deveaud-Plédran, *Nat Mater* **9**, 655 (2010), 10.1038/nmat2787.
  - <sup>6</sup> C. Ciuti, P. Schwendimann, and A. Quattropani, *Phys. Rev. B* **63**, 041303 (2001).
  - <sup>7</sup> D. M. Whittaker, *Phys. Rev. B* **63**, 193305 (2001).
  - <sup>8</sup> N. A. Gippius, S. G. Tikhodeev, V. D. Kulakovskii, D. N. Krizhanovskii, and A. I. Tartakovskii, *EPL* **67**, 997 (2004).
  - <sup>9</sup> D. N. Krizhanovskii, D. M. Whittaker, R. A. Bradley, K. Guda, D. Sarkar, D. Sanvitto, L. Vina, E. Cerda, P. Santos, K. Biermann, R. Hey, and M. S. Skolnick, *Phys. Rev. Lett.* **104**, 126402 (2010).
  - <sup>10</sup> D. Sanvitto, F. M. Marchetti, M. H. Szymanska, G. Tosi, M. Baudisch, F. P. Laussy, D. N. Krizhanovskii, M. S. Skolnick, L. Marrucci, A. Lemaître, J. Bloch, C. Tejedor, and L. Vina, *Nat Phys* **6**, 527 (2010), 10.1038/nphys1668.
  - <sup>11</sup> D. N. Krizhanovskii, S. S. Gavrilov, A. P. D. Love, D. Sanvitto, N. A. Gippius, S. G. Tikhodeev, V. D. Kulakovskii, D. M. Whittaker, M. S. Skolnick, and J. S. Roberts, *Phys. Rev. B* **77**, 115336 (2008).
  - <sup>12</sup> A. A. Demenev, A. A. Shchekin, A. V. Larionov, S. S. Gavrilov, V. D. Kulakovskii, N. A. Gippius, and S. G. Tikhodeev, *Phys. Rev. Lett.* **101**, 136401 (2008).
  - <sup>13</sup> J. Kasprzak, M. Richard, S. Kundermann, A. Baas, P. Jeambrun, J. M. J. Keeling, F. M. Marchetti, M. H. Szymanska, R. André, J. L. Staehli, V. Savona, P. B. Littlewood, B. Deveaud, and L. S. Dang, *Nature* **443**, 409 (2006), 10.1038/nature05131.
  - <sup>14</sup> I. A. Shelykh, T. C. H. Liew, and A. V. Kavokin, *Phys. Rev. Lett.* **100**, 116401 (2008).
  - <sup>15</sup> T. C. H. Liew, A. V. Kavokin, and I. A. Shelykh, *Phys. Rev. Lett.* **101**, 016402 (2008).
  - <sup>16</sup> S. S. Gavrilov, N. A. Gippius, S. G. Tikhodeev, and V. D. Kulakovskii, *JETP* **110**, 825 (2010).
  - <sup>17</sup> D. Sarkar, S. S. Gavrilov, M. Sich, J. H. Quilter, R. A. Bradley, N. A. Gippius, K. Guda, V. D. Kulakovskii, M. S. Skolnick, and D. N. Krizhanovskii, *Phys. Rev. Lett.* **105**, 216402 (2010).
  - <sup>18</sup> C. Adrados, A. Amo, T. C. H. Liew, R. Hivet, R. Houdré, E. Giacobino, A. V. Kavokin, and A. Bra-mati, *Phys. Rev. Lett.* **105**, 216403 (2010).
  - <sup>19</sup> A. A. Demenev, S. S. Gavrilov, and V. D. Kulakovskii, *Phys. Rev. B* **81**, 035328 (2010).
  - <sup>20</sup> P. Renucci, T. Amand, X. Marie, P. Senellart, J. Bloch, B. Sermage, and K. V. Kavokin, *Phys. Rev. B* **72**, 075317 (2005).
  - <sup>21</sup> D. N. Krizhanovskii, D. Sanvitto, I. A. Shelykh, M. M. Glazov, G. Malpuech, D. D. Solnyshkov, A. Kavokin, S. Ceccarelli, M. S. Skolnick, and J. S. Roberts, *Phys. Rev. B* **73**, 073303 (2006).
  - <sup>22</sup> J. ichi Inoue, T. Brandes, and A. Shimizu, *Phys. Rev. B* **61**, 2863 (2000).
  - <sup>23</sup> M. Wouters, *Phys. Rev. B* **76**, 045319 (2007).
  - <sup>24</sup> S. Schumacher, N. H. Kwong, and R. Binder, *Phys. Rev. B* **76**, 245324 (2007).
  - <sup>25</sup> M. Vladimirova, S. Cronenberger, D. Scalbert, K. V. Kavokin, A. Miard, A. Lemaître, J. Bloch, D. Solnyshkov, G. Malpuech, and A. V. Kavokin, *Phys. Rev. B* **82**, 075301 (2010).
  - <sup>26</sup> M. Kuwata-Gonokami, S. Inouye, H. Suzuura, M. Shirane, R. Shimano, T. Someya, and H. Sakaki, *Phys. Rev. Lett.* **79**, 1341 (1997).
  - <sup>27</sup> The experiments of Ref. 19 were performed under the time-resolved nanosecond long excitation at the magic angle. Further, the relation  $W_{\text{thr}}^{(\text{lin})} < W_{\text{thr}}^{(\text{circ})}$  was observed under normal incidence cw excitation in the  $3\mu\text{m}$  wide cavity mesa<sup>5</sup> and (under the same cw pump conditions) in ordinary (spatially uniform) microcavity structure.<sup>17</sup> In the latter case, the negative sign of  $V_2$  in a studied sample was proven by the observed rotation of the scattering signal polarization. In the case of weakly circularly polarized pump, the jumps in both  $\sigma^+$  and  $\sigma^-$  modes were found to occur simultaneously<sup>5,17</sup> in the sense of cw excitation conditions with “infinitesimally slow” variations of pump intensity. In view of the Gross-Pitaevskii equations (1)–(4), this looks like a manifestation of a large repulsion between polaritons with opposite pseudospins. At the same time, in a case when the pump energy is less than a half of biexciton energy, one expects an attractive interaction between excitons with different pseudospins,<sup>23</sup> so they cannot provide blueshift for each other; it agrees with the observed indications of the negative sign of  $V_2$ .
  - <sup>28</sup> E. A. Cerda-Méndez, D. N. Krizhanovskii, M. Wouters, R. Bradley, K. Biermann, K. Guda, R. Hey, P. V. Santos, D. Sarkar, and M. S. Skolnick, *Phys. Rev. Lett.* **105**, 116402 (2010).
  - <sup>29</sup> S. S. Gavrilov, A. S. Brichtkin, A. A. Dorodny, S. G. Tikhodeev, N. A. Gippius, and V. D. Kulakovskii, *JETP Lett.* **92** (2010).
  - <sup>30</sup> M. Wouters and I. Carusotto, *Phys. Rev. Lett.* **99**, 140402 (2007).

<sup>31</sup> For the sake of simplicity, only the nonlinear mechanism of reservoir population ( $\gamma_{\text{sr}} = 0$  and  $V_{\text{r}} \neq 0$ ) has been considered in Ref. 17. In such a case, the reservoir induced blueshifts are determined mainly by the ratio between reservoir's decay rate and the coupling constant  $V_{\text{r}}$ . For instance, the calculations performed with different  $\gamma_{\text{r}}$  but constant  $\gamma_{\text{r}}/V_{\text{r}}$  and a sufficiently slow variation of the pump power lead to exactly same results for the cases of circular and linear pump polarizations. In this connection, the experiments carried out with time resolution using the nanosecond long pump pulses (described in Sec. IV) are capable of clarifying the characteristic lifetimes of the reser-

voir states, as well as the relation between linear and nonlinear mechanisms of polaritons' scattering into the incoherent exciton reservoir. For instance, the former mechanism is expected to play a role irrespectively of pump polarization, affecting the dynamics of polariton energy and the time moments when the nonequilibrium transitions occur.

<sup>32</sup> S. G. Tikhodeev, A. L. Yablonskii, E. A. Muljarov, N. A. Gippius, and T. Ishihara, Phys. Rev. B **66**, 045102 (2002).

<sup>33</sup> A. A. Demenev, A. A. Shchekin, A. V. Lari-onov, S. S. Gavrilov, and V. D. Kulakovskii, Phys. Rev. B **79**, 165308 (2009).